Gauge violation spectroscopy of synthetic gauge theories

Hao-Yue Qi[1,2] and Wei Zheng[1,2,3,*]

[1]*Hefei National Laboratory for Physical Sciences at the Microscale and Department of Modern Physics, University of Science and Technology of China, Hefei 230026, China*

[2]*CAS Center for Excellence in Quantum Information and Quantum Physics, University of Science and Technology of China, Hefei 230026, China*

[3]*Hefei National Laboratory, University of Science and Technology of China, Hefei 230088, China*

(Received 29 August 2023; accepted 14 December 2023; published 12 January 2024)

Recently synthetic gauge fields have been implemented on quantum simulators. Unlike the gauge fields in the real world, in synthetic gauge fields, the gauge charge can fluctuate and gauge invariance can be violated, which leads to rich physics unexplored before. In this work, we first propose the gauge violation spectroscopy as a powerful experimentally accessible measurement of synthetic gauge theories. We show that the gauge violation spectroscopy exhibits no dispersion. Using three models as examples, two of which can be exactly solved by bosonization, and one that has been realized in experiment, we further demonstrate the gauge violation spectroscopy can be used to detect the confinement and deconfinement phases. In the confinement phase, it shows a δ-function behavior, while in the deconfinement phase, it has a finite width.

DOI: 10.1103/PhysRevResearch.6.013047

I. INTRODUCTION

Gauge theories play a central role in modern physics. On one hand, gauge theories provide a unified description of fundamental interactions between elementary particles within the standard model [1]. On the other hand, gauge fields emerge from the low-energy effective theories of strongly correlated condensed matter [2,3]. Despite the success of gauge theories, studying the real-time dynamics of gauge fields is a notable challenge due to the limit of the classical computational methods. To overcome these limitations, synthetic gauge fields have been implemented on quantum simulators based on ultracold atoms in optical lattices [4–11], trapped ions [12], or superconducting qubits [13,14].

The key concept of gauge theories is the local gauge symmetry, $[\hat{G}(\mathbf{r}), \hat{H}] = 0$, where $\hat{G}(\mathbf{r})$ is the local gauge transformation and $\hat{H}$ is the Hamiltonian of the system. Local gauge symmetry separates the Hilbert space into disconnected sectors labeled by local gauge charge $\hat{Q}(\mathbf{r})$, the generator of $\hat{G}(\mathbf{r})$, see Fig. 1. In the real world, we are living in the so-called physical sector with vanishing gauge charge $\hat{Q}(\mathbf{r}) = 0$. Projecting into physical sector enforces an extensive number of local constrains between matter and gauge fields, which is nothing but the Gaussian law. However, in synthetic gauge theories on quantum simulators, local gauge charge $\hat{Q}(\mathbf{r})$ is not restricted to the physical sector. It can even fluctuate due to intersector superposition or gauge violation perturbations and noise [15,16]. To simulate the real gauge theories in the physical sector, one has to carefully prepare gauge invariant initial states, i.e., states in the physical sector and suppress the unwanted gauge violation perturbations and noise. That stimulates the seeking of local gauge protection schemes [17,18]. However, such fluctuations of gauge charges can lead to richer gauge violation physics. For example, disorder-free localization can emerge in synthetic gauge theories by preparing the initial states as the superposition of several sectors [19–25]. Besides, allowing transitions between different sectors can also lead to exotic phase transition that does not exist in real gauge theories [26,27].

Spectroscopy measurement is a powerful technique to detect the excitations in both real materials and quantum simulators. It has been widely used to probe the spectrums of single-particle and collective excitations, which determine the phases and dynamics of a given quantum system. For example, the angle-resolved photoemission spectroscopy (ARPES) [28] has been applied to study the pseudogap of high-T_c cuprates and edge states of topological insulators. In ultracold atomic gases, radio frequency (RF) spectroscopy [29] is used to measure single-particle spectrums of Fermi gases [30–34] and Fermi/Bose polarons [35–39]. Several spectroscopy techniques have also been developed in other quantum simulation platforms, such as trapped ions [40,41] and superconducting qubits [42]. However, the spectroscopy study of synthetic gauge theories on quantum simulators is still missing.

In this paper, we first propose the gauge violation spectroscopy a powerful experimentally accessible tool to probe the synthetic gauge theories on quantum simulators. By gauge violation, we mean that the measurement induces a transition

*zw8796@ustc.edu.cn

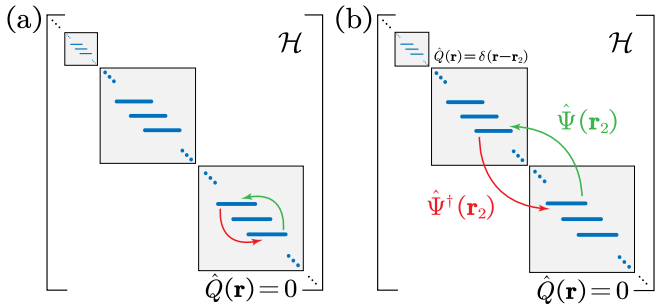

FIG. 1. Schematic of (a) gauge invariance and (b) violation spectroscopy. The blocks represent different gauge sectors labeled by $\hat{Q}(\mathbf{r})$ in Hilbert space. In the gauge violation case (b), the operations $\hat{\Psi}(\mathbf{r}_2)$, $\hat{\Psi}^\dagger(\mathbf{r}_2)$ induce a transition between $\hat{Q}=0$ and $\hat{Q}=\delta(\mathbf{r}-\mathbf{r}_2)$ gauge sectors.

between different gauge sectors, see Fig. 1. We demonstrate that the usual single-particle spectroscopy measurement process (such as RF spectroscopy in ultracold atomic gases) of synthetic gauge theories is gauge violation rather than gauge invariant. Besides, the gauge invariant spectroscopy needs highly nonlocal probes, and is challenging in current experiments. Furthermore, we show that the gauge violation spectroscopy exhibits no dispersion, as it violates the Gauss law. Using three models that possess local $U(1)$ gauge symmetries as examples, we show that the gauge violation spectroscopy can be used to detect the confinement and deconfinement phases in gauge theories. In the confinement phase, gauge violation spectrum is nearly a δ function, while in the deconfinement phase, it exhibits a finite width.

The rest of this paper is organized as follows. We introduce the basic concept of gauge violation spectroscopy in Sec. I. Then we calculate the gauge violation spectrum of two Schwinger-like models by bosonization method in Sec. III. We calculate the gauge violation spectrum of a quantum link model, which has been realized recently in Sec. IV. In Sec. V, we summarize the results.

II. BASIC CONCEPT OF GAUGE VIOLATION SPECTROSCOPY

As we know the single-particle absorbing and emission spectrum function can be obtained from the Fourier transformation of the following Green's functions:

$$\mathcal{A}_{\rm ab}(\mathbf{k},\omega)=i\int dt\int d\mathbf{r}g^{>}_{\mathbf{r}}(t)e^{-i(\mathbf{k}\cdot\mathbf{r}-\omega t)}, \tag{1}$$

$$\mathcal{A}_{\rm em}(\mathbf{k},\omega)=i\varepsilon\int dt\int d\mathbf{r}g^{<}_{\mathbf{r}}(t)e^{-i(\mathbf{k}\cdot\mathbf{r}-\omega t)}. \tag{2}$$

These Green's functions are defined as

$$ig^{>}_{\mathbf{r}_2-\mathbf{r}_1}(t)=\langle\psi_0|\hat{\Psi}(\mathbf{r}_2,t)\hat{\Psi}^\dagger(\mathbf{r}_1,0)|\psi_0\rangle, \tag{3}$$

$$ig^{<}_{\mathbf{r}_2-\mathbf{r}_1}(t)=\varepsilon\langle\psi_0|\hat{\Psi}^\dagger(\mathbf{r}_1,0)\hat{\Psi}(\mathbf{r}_2,t)|\psi_0\rangle, \tag{4}$$

where $\hat{\Psi}(\mathbf{r},t)=e^{iHt}\hat{\Psi}(\mathbf{r})e^{-iHt}$ is the matter field operator in Heisenberg picture, and $\varepsilon=+1(-1)$ for bosonic (fermionic) matter field. Here we choose $|\psi_0\rangle$ to be the ground state in the physical sector, i.e., the sector with vanishing gauge charge $\hat{Q}(\mathbf{r})=0$. These Green's functions describe the process that adding one particle (hole) to the system at position $\mathbf{r}_1$, and removing one particle (hole) at position $\mathbf{r}_2$ after evolution time t. In synthetic gauge theories, the gauge field can not adjust to follow the charge we add (remove). Thus this process violates the Gaussian law, and excites the system away from the physical sector. More specifically, matter field operator is not invariant under local gauge transformation, thus $[\hat{\Psi}^{(\dagger)}(\mathbf{r}'),\hat{Q}(\mathbf{r})]\neq 0$. One finds

$$\hat{Q}(\mathbf{r})\hat{\Psi}^{(\dagger)}(\mathbf{r}')|\psi_0\rangle=\pm e\delta(\mathbf{r}-\mathbf{r}')\hat{\Psi}^{(\dagger)}(\mathbf{r}')|\psi_0\rangle. \tag{5}$$

Note that the state $\hat{\Psi}^{(\dagger)}(\mathbf{r}')|\psi_0\rangle$ is no longer in the physical sector as shown in Fig. 1(b), but in the sector with gauge charge $\hat{Q}(\mathbf{r})=\xi e\delta(\mathbf{r}-\mathbf{r}_1)$. Then the Green's functions can be simplified into

$$ig^{>}_{\mathbf{r}_2-\mathbf{r}_1}(t)=\delta(\mathbf{r}_2-\mathbf{r}_1)\langle\psi_0|\hat{\Psi}(\mathbf{r}_2)e^{-i\hat{H}_- t}\hat{\Psi}^\dagger(\mathbf{r}_1)|\psi_0\rangle, \tag{6}$$

$$ig^{<}_{\mathbf{r}_2-\mathbf{r}_1}(t)=\varepsilon\delta(\mathbf{r}_2-\mathbf{r}_1)\langle\psi_0|\hat{\Psi}^\dagger(\mathbf{r}_1)e^{+i\hat{H}_+ t}\hat{\Psi}(\mathbf{r}_2)|\psi_0\rangle, \tag{7}$$

where $\hat{H}_\xi\equiv\hat{H}[\hat{Q}(\mathbf{r})=\xi e\delta(\mathbf{r}-\mathbf{r}_1)]$, $\xi=\pm$, is the Hamiltonian in the unphysical sectors, and energy of $|\psi_0\rangle$ is set to be zero. Here the δ function $\delta(\mathbf{r}_2-\mathbf{r}_1)$ is due to the fact that if $\mathbf{r}_2\neq\mathbf{r}_1$, the state will not go back to the physical sector, $\hat{Q}(\mathbf{x})\hat{\Psi}(\mathbf{r}_2)\hat{\Psi}^\dagger(\mathbf{r}_1)|\psi_0\rangle=\{\delta(\mathbf{x}-\mathbf{r}_2)-\delta(\mathbf{x}-\mathbf{r}_1)\}\hat{\Psi}(\mathbf{r}_2)\hat{\Psi}^\dagger(\mathbf{r}_1)|\psi_0\rangle$. As a result, the gauge violation spectrum exhibits no dispersion,

$$\mathcal{A}_{\rm ab/em}(\mathbf{k},\omega)=\mathcal{A}_{\rm ab/em}(\omega). \tag{8}$$

In contrast to gauge violation spectroscopy, to calculate the gauge invariant spectrum, one needs to bind the matter field operator to the gauge fields

$$\hat{\Psi}(\mathbf{r})\longrightarrow\hat{\Psi}(\mathbf{r})e^{i\int d^dx\mathbf{E}_{\rm cl}(\mathbf{x})\cdot\hat{\mathbf{A}}(\mathbf{x})}, \tag{9}$$

where $\mathbf{E}_{\rm cl}(\mathbf{x})$ is a classical electric field satisfying $\nabla\cdot\mathbf{E}_{\rm cl}(\mathbf{x})=\delta(\mathbf{x}-\mathbf{r})$. It is invariant under gauge transformation, and commutes with the gauge charge $[\hat{Q}(\mathbf{r}),\hat{\Psi}(\mathbf{r}')e^{i\int d^dx\mathbf{E}_{\rm cl}(\mathbf{x})\cdot\hat{\mathbf{A}}(\mathbf{x})}]=0$. We note that in most quantum simulators of synthetic gauge theories, it is hard to perform the gauge invariant spectroscopy. Since it is challenging to excite such highly nonlocal excitations. Therefore the commonly used techniques, such as RF spectroscopy, probe the gauge violation spectrum rather than gauge invariant spectrum. Furthermore, we will show that the gauge violation spectroscopy can be used to detect the confinement and deconfinement phases in synthetic gauge theories.

III. TWO SCHWINGER-LIKE MODELS

In the following, we will present two one-dimensional models with $U(1)$ local gauge symmetry, which can be both exactly solved via bosonization method. One is the celebrated Schwinger model. Its Hamiltonian is given by

$$\hat{H}^{\rm c}=\hat{H}_{\rm mat}+\frac{1}{2}\int dx\hat{E}^2(x), \tag{10}$$

where

$$\hat{H}_{\rm mat}=\int dx\hat{\Psi}^\dagger(x)\sigma_z[-i\partial_x-e\hat{A}(x)]\hat{\Psi}(x), \tag{11}$$

and the fermion fields have two components $\hat{\Psi} = (\hat{\Psi}_R, \hat{\Psi}_L)^T$. The Schwinger model describes the (1+1)-dimensional QED [43,44], and exhibits charge confinement phenomena. Another is similar to the Schwinger model. Its Hamiltonian is given by

$$\hat{H}^d = \hat{H}_{\text{mat}} + \frac{u}{2}\int dx[\partial_x \hat{E}(x)]^2. \tag{12}$$

Note that it possesses a modified Maxwell term. The corresponding energy density of gauge field is proportional to the square of electrical field gradient rather than the square of electrical field. This modified Maxwell leads to the deconfinement of charges in this model.

These two models possess the local $U(1)$ gauge symmetries. The corresponding gauge transformation operators are both

$$\begin{aligned}\hat{G} &= \exp\left\{i\int dx[e\hat{\rho}(x)\theta(x) + \hat{E}(x)\partial_x\theta]\right\}\\ &= \exp\left\{ie\int dx\theta(x)[\hat{\rho}(x) - \frac{1}{e}\partial_x\hat{E}(x)]\right\}\\ &= \exp\left\{-ie\int dx\theta(x)\hat{Q}(x)\right\},\end{aligned} \tag{13}$$

where $\theta(x)$ is an arbitrary phase distribution function, and $\hat{\rho}(x) = \hat{\Psi}^\dagger(x)\hat{\Psi}(x)$ is the particle density operator. The generator of this gauge transformation is given by

$$\hat{Q}(x) = \partial_x\hat{E}/e - \hat{\rho}(x). \tag{14}$$

Since $[\hat{G}, \hat{H}^{c(d)}] = 0$, $\hat{Q}(x)$ is a conserved quantity called gauge charge. In the physical sector, $\hat{Q}(x) = 0$, the conservation leads to the Gaussian law in one dimension, $\partial_x\hat{E} = e\hat{\rho}(x)$.

We use the bosonization method to deal with these two models. Bosonization method maps one-dimensional fermions to a problem of bosonic fields [45]. Here both $\hat{H}^c$ and $\hat{H}^d$ can be bosonized in arbitrary gauge sector. As discussed above we only focus on the sector with gauge charge $\hat{Q}(x) = \xi\delta(x - x')$. The corresponding bosonized Hamiltonian in this sector is given by [49],

$$\hat{H}^c_\xi = \hat{H}_{\text{mat}} + \frac{m^2}{2}\int dx\left(\phi + \frac{\xi e\,\text{sgn}(x-x')}{2m}\right)^2, \tag{15}$$

$$\hat{H}^d_\xi = \hat{H}_{\text{mat}} + \frac{g}{2}\int dx\left(\partial_x\phi + \frac{\xi e\delta(x-x')}{m}\right)^2, \tag{16}$$

where

$$\hat{H}_{\text{mat}} = \frac{1}{2}\int dx[\Pi^2 + (\partial_x\phi)^2], \tag{17}$$

$g = um^2$ and $m^2 = e^2/\pi$. Note that all of these Hamiltonians are quadratic, thus can be exactly diagonalized. Then it is straightforward to calculate the gauge violation correlations defined in Eqs. (6), (7). For the deconfinement model, one obtains [49]

$$ig^>(x,t) = \frac{\delta(x)}{2\pi a}\left(\frac{-ia}{vt - ia}\right)^\gamma e^{-iE_Q t}, \tag{18}$$

$$ig^<(x,t) = \frac{\delta(x)}{2\pi a}\left(\frac{ia}{vt + ia}\right)^\gamma e^{iE_Q t}, \tag{19}$$

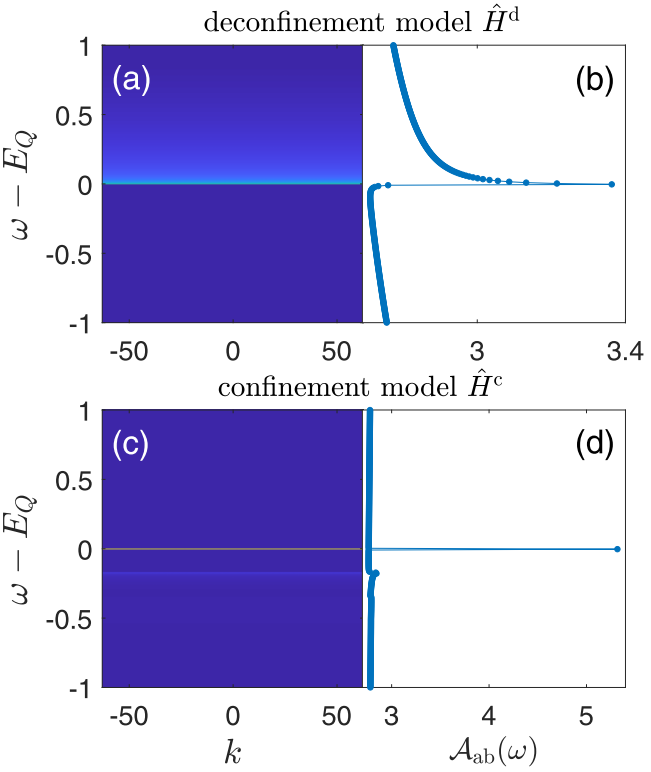

FIG. 2. Gauge violation single-particle absorbing spectrum for (a), (b) deconfinement model and for (c), (d) confinement model. (a), (c) Momentum resolved gauge violation spectrum. (b), (d) Gauge violation spectrum at a given momentum. We have set coupling constant $g = 0.5$ for deconfinement model, and the boson mass $m = e/\sqrt{\pi} = 0.17$ for confinement model.

where $v = \sqrt{1+g}$ and $\gamma = \frac{v^2+1}{2v^3}$. The ultraviolet cutoff a is introduced by the bosonization procedure, and E_Q is an unimportant constant energy. For the Schwinger model, it is hard to obtain a compact analytic form [49]. Then performing the Fourier transformation one obtains the gauge violation spectral functions.

The results are shown in Figs. 2 and 3. Note that for both models, the gauge violation spectrums exhibit no dispersion. For the model with charge confinement, the gauge violation spectrum is a δ function. By contrast, for the deconfined model, the gauge violation spectrum has a finite width. This behavior can be understood as follows: The gauge violation spectroscopy measurement adds one particle with charge $+e$ into the system, and creates a gauge charge $-e$ at the same position, which can not move. The interaction between this particle and the gauge charge is governed by electrical field. In the Schwinger model, this interaction energy is proportional to the length of separation between the added particle and the gauge charge, i.e., it is in the confinement phase. Thus the added particle can not move far away from the original position. However, in the deconfinement model, the interaction energy is nearly a constant. Then the added particle can move away from the original position. For comparison, we also have calculated the gauge invariance spectroscopy in the Appendix B, which exhibits linear dispersion in momentum space.

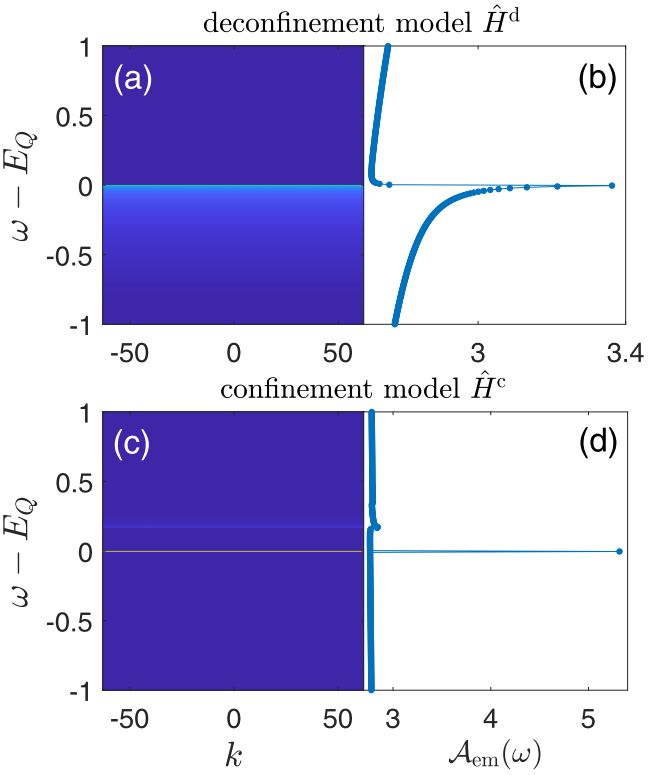

FIG. 3. Gauge violation single-particle emission spectrum for (a), (b) deconfinement model and for (c), (d) confinement model. (a), (c) Momentum-resolved gauge violation spectrum. (b), (d) Gauge violation spectrum at a given momentum. We have set coupling constant $g = 0.5$ for deconfinement model, and the boson mass $m = e/\sqrt{\pi} = 0.17$ for confinement model.

IV. QUANTUM LINK MODEL

Recently, the one-dimensional quantum link model, a $U(1)$ lattice gauge theory, has been realized on a quantum simulator based on ultracold bosons in optical lattices [5]. The Gauss law, as well as the thermalization of this model have been observed [7]. By further engineering a tunable topological θ term, confinement-deconfinement transition has been observed [11]. The Hamiltonian of the quantum link model is given by [46,47]

$$\hat{H}_{\mathrm{QLM}} = J\sum_j \left(\hat{\Psi}^\dagger_{j+1}\hat{S}^-_{j+1;j}\hat{\Psi}^\dagger_j + \mathrm{H.c.}\right) + \sum_j M\hat{\Psi}^\dagger_j\hat{\Psi}_j + \chi\sum_j (-1)^j \hat{S}^z_{j+1;j}. \quad (20)$$

Here the gauge field is represented by spin-1/2 operators $\hat{S}^+_{i+1;i}$ on links. The matter fields $\hat{\Psi}_j$ on even and odd sites represent particles and antiparticles. Thus, the term $\hat{\Psi}^\dagger_{j+1}\hat{S}^-_{j+1;j}\hat{\Psi}\dagger_j$ represents the process of generating particle-antiparticle pairs, as annihilating gauge fields. J is the gauge-matter coupling strength and M is the mass of the matter field. χ can tune the topological theta angle θ. When $\chi = 0$, $\theta = \pi$, as $\chi \neq 0$, θ is tuned away from π. When $\chi \neq 0$, i.e., θ is away from π, it is in the confined phase, and no single charge can be observed. When $\chi = 0$, i.e., $\theta = \pi$, there is a transition from confined phase to deconfined phase by tuning the matter mass from negative to positive.

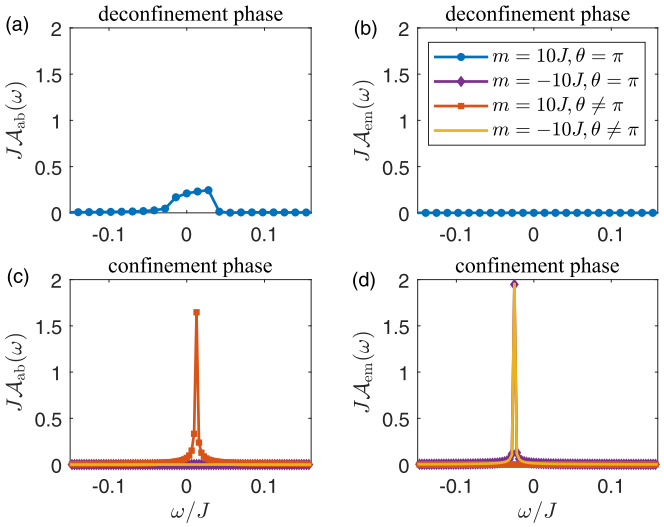

FIG. 4. Gauge violation spectroscopies for the one-dimensional quantum link model. (a), (b) Results for deconfinement phase with $M = 10J, \theta = \pi$. (c), (d) Results for confinement phase with $M = -10J, \theta = \pi$ and $M = \pm 10J, \theta = \pi/2$. The model contains total number of sites $L = 20$.

The local gauge transformation operator is $\hat{G}_j = e^{i\phi\hat{Q}_j}$, and the conserved gauge charge is $\hat{Q}_j = \hat{S}^z_{j+1;j} + \hat{S}^z_{j;j-1} + \hat{\Psi}^\dagger_j\hat{\Psi}_j$. We calculate the gauge violation spectrum by numerical exact diagonalization. The results of numerical simulation are shown in Fig. 4. In Figs. 4(a)–4(b), we observe the deconfinement behavior with $M = 10J$ and the topological angle $\theta = \pi$. The spectrum has a finite width. Instead, Figs. 4(c)–4(d) show the confinement behavior with $M = -10J, \theta = \pi$. It shows the δ-function behavior. This difference clearly distinguishes confinement from deconfinement phase. In Figs. 4(c)–4(d), we also observe the same δ-function behavior with $M = \pm 10J, \theta \neq \pi$, because there is only a confinement phase when $\theta \neq \pi$.

V. SUMMARY

We propose the gauge violation spectroscopy in synthetic gauge theories on quantum simulators, which could be used to detect the confinement phase or deconfinement phase. In most single-particle spectroscopy of synthetic gauge theories, such as RF spectroscopy in ultracold quantum gases, one measured the gauge violation spectrum, rather than the gauge invariant spectrum. Since later spectroscopy needs highly nonlocal perturbations. We used three one-dimensional models with local $U(1)$ gauge symmetry to show that in the confined phase, the gauge violation spectrum is nearly a δ function, while in the deconfinement phase the spectrum has a finite width. However, our conclusions are not limited to one-dimensional models with $U(1)$ gauge symmetry. It can be applied to higher dimension or non-Abelian gauge. In addition, we would like to point out that, for some simulators, the projected Hamiltonian instead of the Hamiltonian in the full Hilbert space is realized [48]. In this situation, there is no room for fluctuation

of gauge charge. Thus the gauge violation spectroscopy can not be applied in these simulators.

ACKNOWLEDGMENTS

We thank H. Zhai and Y. Cheng for discussion. This work is supported by NSFC (Grants No. GG2030007011 and No. GG2030040453) and Innovation Program for Quantum Science and Technology (Grants No. 2021ZD0302000 and No. 2021ZD0302004).

APPENDIX A: BOSONIZATION OF SCHWINGER-LIKE MODELS

To calculate the spectral functions, we use the bosonization method to deal with two Schwinger-like models Eqs. (10), (12). The bosonization dictionary is given by

$$\hat{\Psi}_{R(L)}(x) \to \frac{1}{\sqrt{2\pi a}} e^{(-)i\sqrt{4\pi}\hat{\phi}_{R(L)}(x)}, \tag{A1}$$

$$\hat{\rho}(x) = \hat{\Psi}_R^\dagger \hat{\Psi}_R + \hat{\Psi}_L^\dagger \hat{\Psi}_L \to \frac{1}{\sqrt{\pi}} \partial_x \hat{\phi}, \tag{A2}$$

$$\begin{aligned} \hat{H}_{\text{mat}} &= \int dx \hat{\Psi}^\dagger(x) \sigma_z [-i\partial_x - e\hat{A}(x)] \hat{\Psi}(x), \\ &\to \frac{1}{2} \int dx [\hat{\Pi}^2 + (\partial_x \hat{\phi})^2], \end{aligned} \tag{A3}$$

and some definitions in the above equations

$$\hat{\phi} = \hat{\phi}_R + \hat{\phi}_L, \tag{A4}$$

$$\hat{\theta} = \hat{\phi}_L - \hat{\phi}_R, \tag{A5}$$

$$\hat{\Pi}(x) = \partial_x \hat{\theta}(x). \tag{A6}$$

$$\hat{\phi}_R(x) = \sum_q \frac{\Theta(+q)}{\sqrt{2L|q|}} \left(\hat{b}_q e^{iqx} + \hat{b}_q^\dagger e^{-iqx}\right), \tag{A7}$$

$$\hat{\phi}_L(x) = \sum_q \frac{\Theta(-q)}{\sqrt{2L|q|}} \left(\hat{b}_q e^{iqx} + \hat{b}_q^\dagger e^{-iqx}\right), \tag{A8}$$

where $\hat{b}_q$ is the usual bosonic annihilation operator in the state with momentum q satisfying the commutation relations $[\hat{b}_q, \hat{b}_{q'}^\dagger] = \delta_{qq'}$. $e^{-aq/2}$ is a converging factor with $a \to 0^+$. The system size L will be set to infinity in the last step.

It is straightforward to bosonize the first term in the two models Eqs. (10), (12). Thus, let us focus on the second term, which includes the electric field. We can work out the electric field $\hat{E}(x)$ from Gauss law (14) using Green's function method,

$$\hat{E}(x) = \int dy \frac{e}{2} [\Theta(x-y) - \Theta(y-x)][\hat{Q}(y) + \hat{\rho}(x)]\, dy. \tag{A9}$$

Then use the bosonic expression of $\hat{\rho}(x)$, and straightforward integration leads to

$$\hat{E}(x) = \hat{E}_B(x) + \frac{e}{\sqrt{\pi}} \hat{\phi}(x), \tag{A10}$$

where the background electric field generated by the gauge charge $Q(x)$ is defined as

$$\hat{E}_B(x) = \int dy \frac{e}{2} \text{sgn}(x-y) \hat{Q}(y) dy. \tag{A11}$$

Take the spatial derivative on both sides of Eq. (A10), and we have

$$\partial_x \hat{E}(x) = e\hat{Q}(x) + \frac{e}{\sqrt{\pi}} \partial_x \hat{\phi}(x). \tag{A12}$$

Substitute Eq. (A10) and (A12) into Eqs. (10) and (12), respectively, and we arrive at the bosonized Hamiltonians in any sector $\hat{Q}(x)$ for the Schwinger-like models,

$$\begin{aligned} \hat{H}^{\text{c}} &= \frac{1}{2} \int dx \left[\hat{\Pi}^2 + (\partial_x \hat{\phi})^2\right], \\ &\quad + \frac{1}{2} m^2 \int dx \left(\frac{\sqrt{\pi}}{e} \hat{E}_B(x) + \hat{\phi}(x)\right)^2 \end{aligned} \tag{A13}$$

$$\begin{aligned} \hat{H}^{d} &= \frac{1}{2} \int dx \left[\hat{\Pi}^2 + (\partial_x \hat{\phi})^2\right] \\ &\quad + \frac{1}{2} g \int dx (\sqrt{\pi} \hat{Q}(x) + \partial_x \hat{\phi})^2 \end{aligned} \tag{A14}$$

with the mass of the bosonic field $\hat{\phi}$, $m^2 = \frac{e^2}{\pi}$, and a dimensionless coupling constant $g = ue^2/\pi$. In sectors $\hat{Q}(x) = \xi \delta(x - x')$ with $\xi = 0, \pm$, we obtain $\hat{H}_\xi^{\text{c(d)}}$ in the main text.

APPENDIX B: SPECTRAL FUNCTIONS

In the following, we want to calculate the following types of correlations:

$$ig_\sigma^>(x,t) = \langle \psi_0 | \hat{\Psi}_R(x) e^{-i\hat{H}_\xi^\sigma t} \hat{\Psi}_R^\dagger(0) | \psi_0 \rangle e^{+iE_0^\sigma t}, \tag{B1}$$

$$ig_\sigma^<(x,t) = \langle \psi_0 | \hat{\Psi}_R^\dagger(0) e^{+i\hat{H}_\xi^\sigma t} \hat{\Psi}_R(x) | \psi_0 \rangle e^{-iE_0^\sigma t}. \tag{B2}$$

Here, $\hat{H}_\xi^\sigma$ with $\sigma = \text{c}, \text{d}$ denote the Hamiltonians of Schwinger-like models as in the main text or see Eqs. (B3), (B4). The two models can be discussed in a fully parallel and unified fashion by introducing the parameter σ. The $|\psi_0\rangle$ and E_0^σ are the ground state and energy in the physical sector, $\hat{H}_{\xi=0}^\sigma |\psi_0\rangle = E_0^\sigma |\psi_0\rangle$. Since the right and left movers possess the same physics as the other, we only focus on the right mover in the following.

First, we diagonalize the bosonic Schwinger-like models in sectors $\hat{Q}(x) = \xi \delta(x)$ with $\xi = 0, \pm$,

$$\hat{H}_\xi^d = \hat{H}_{\text{mat}} + \frac{m^2}{2} \int dx \left[\phi + \frac{\xi e \text{sgn}(x)}{2m}\right]^2, \tag{B3}$$

$$\hat{H}_\xi^{\text{c}} = \hat{H}_{\text{mat}} + \frac{g}{2} \int dx \left[\partial_x \phi + \frac{\xi e \delta(x)}{m}\right]^2. \tag{B4}$$

It is important to note that the definition of the bosonic field Eq. (A4) and the Fourier expansion of $\text{sgn}(x) = \frac{1}{L} \sum_k \frac{2}{ik} e^{ikx}$ allow us to rewrite the Hamiltonians into a unified form in momentum space

$$\begin{aligned} \hat{H}_\xi^\sigma &= E_{\text{zp}}^\sigma + \xi^2 E_Q^\sigma + \sum_q \Big[\mu_q^\sigma \hat{b}_q^\dagger \hat{b}_q + \frac{1}{2} \Omega_q^\sigma \left(\hat{b}_q \hat{b}_{-q} + \hat{b}_{-q}^\dagger \hat{b}_q^\dagger\right) \\ &\quad + i\xi \lambda_q^\sigma \left(\hat{b}_q - \hat{b}_q^\dagger\right)\Big]. \end{aligned} \tag{B5}$$

Here,

$$E_{\rm zp}^{\rm c}=\sum_q\frac{1}{2}\left(|q|+\frac{m^2}{2|q|}\right)\quad E_{\rm zp}^{d}=\sum_q\frac{1}{2}\left(1+\frac{g}{2}\right)|q|,$$
$$E_Q^{\rm c}=\sum_q\frac{e^2}{2Lq^2}\quad E_Q^{d}=\sum_q\frac{e^2g}{2Lm^2},$$
$$\mu_q^{\rm c}=|q|+\frac{m^2}{2|q|}\quad \mu_q^{d}=\left(1+\frac{g}{2}\right)|q|,$$
$$\Omega_q^{\rm c}=\frac{m^2}{2|q|}\quad \Omega_q^{d}=\frac{g|q|}{2},$$
$$\lambda_q^{\rm c}=\frac{em}{q\sqrt{2L|q|}}\quad \lambda_q^{d}=\frac{egq}{m\sqrt{2L|q|}}.$$

So the Hamiltonian in the physical sector is given by

$$\hat{H}_{\xi=0}^{\sigma}=E_{\rm zp}^{\sigma}+\sum_q\left\{\mu_q^{\sigma}\hat{b}_q^{\dagger}\hat{b}_q+\frac{1}{2}\Omega_q^{\sigma}\left(\hat{b}_q\hat{b}_{-q}+\hat{b}_{-q}^{\dagger}\hat{b}_q^{\dagger}\right)\right\},\tag{B6}$$

which can be diagonalized by utilizing the Bogoliubov transformation

$$\hat{b}_q=u_q^{\sigma}\hat{\beta}_q-v_q^{\sigma}\hat{\beta}_{-q}^{\dagger},\quad \hat{b}_q^{\dagger}=u_q^{\sigma}\hat{\beta}_q^{\dagger}-v_q^{\sigma}\hat{\beta}_{-q},$$

with

$$\left(u_q^{\sigma}\right)^2=\frac{1}{2}\left(\frac{\mu_q^{\sigma}}{\varepsilon_q^{\sigma}}+1\right)\quad \left(v_q^{\sigma}\right)^2=\frac{1}{2}\left(\frac{\mu_q^{\sigma}}{\varepsilon_q^{\sigma}}-1\right),$$
$$\varepsilon_q^{\rm c}=\sqrt{|q|^2+m^2}\quad \varepsilon_q^{d}=\sqrt{1+g}|q|.$$

It follows that

$$\hat{H}_{\xi=0}^{\sigma}=E_0^{\sigma}+\sum_q\varepsilon_q^{\sigma}\hat{\beta}_q^{\dagger}\hat{\beta}_q,\tag{B7}$$

where $E_0^{\sigma}=E_{\rm zp}^{\sigma}+E_{\rm LHY}^{\sigma}$ is the ground-state energy in the physical sector, and $E_{\rm LHY}=\frac{1}{2}\sum_q(\varepsilon_q^{\sigma}-\mu_q^{\sigma})$. In this basis, the Hamiltonians in sectors $\hat{Q}(x)=\xi\delta(x)$ can be rewritten into

$$\begin{aligned}\hat{H}_{\xi}^{\sigma}&=E_0^{\sigma}+\xi^2E_Q^{\sigma}+\sum_q\varepsilon_q^{\sigma}\hat{\beta}_q^{\dagger}\hat{\beta}_q\\&\quad+\sum_q i\xi\lambda_q^{\sigma}\left(u_q^{\sigma}-v_q^{\sigma}\right)\left(\hat{\beta}_q-\hat{\beta}_q^{\dagger}\right)\\&=E_0^{\sigma}+\xi^2\tilde{E}_Q^{\sigma}+\sum_q\varepsilon_q^{\sigma}\left(\hat{\beta}_q^{\dagger}+\xi h_q^{\sigma *}\right)\left(\hat{\beta}_q+\xi h_q^{\sigma}\right)\end{aligned}\tag{B8}$$

with

$$h_q^{\sigma}=-i\frac{\lambda_q^{\sigma}}{\varepsilon_q^{\sigma}}\left(u_q^{\sigma}-v_q^{\sigma}\right),\tag{B9}$$
$$\tilde{E}_Q^{\sigma}=E_Q^{\sigma}-\sum_q\left(\lambda_q^{\sigma}\right)^2\left(u_q^{\sigma}-v_q^{\sigma}\right)^2/\varepsilon_q^{\sigma}.\tag{B10}$$

To calculate spectral functions, it is also convenient to rewrite the bosonic fields Eq. (A1) in terms of the new basis

$$\hat{\Psi}_R(x)=\frac{1}{\sqrt{2\pi a}}e^{\sum_q\left[\eta_q^{\sigma}(x)\hat{\beta}_q^{\dagger}-\eta_q^{\sigma *}(x)\hat{\beta}_q\right]}\tag{B11}$$

with

$$\eta_q^{\sigma}(x)=i\sqrt{\frac{2\pi}{|q|L}}\left[\Theta(+q)u_q^{\sigma}-\Theta(-q)v_q^{\sigma}\right]e^{-iqx}.$$

1. Gauge invariance spectroscopy

Substitute Eqs. (B7), (B11) into the Green's function Eq. (B1), and we obtain

$$\begin{aligned}ig_{\sigma}^{>}(x,t)&=\frac{1}{2\pi a}\langle\psi_0|e^{+\sum_q\left[\eta_q^{\sigma}(x)\hat{\beta}_q^{\dagger}-\eta_q^{*\sigma}(x)\hat{\beta}_q\right]}e^{-it\sum_q\varepsilon_q^{\sigma}\hat{\beta}_q^{\dagger}\hat{\beta}_q}\\&\quad\times e^{-\sum_q\left[\eta_q^{\sigma}(0)\hat{\beta}_q^{\dagger}-\eta_q^{*\sigma}(0)\hat{\beta}_q\right]}|\psi_0\rangle,\end{aligned}$$

and $ig_{\sigma}^{<}(x,t)$ is similar. Since we are calculating the correlations for the ground state $|\psi_0\rangle$ of $\hat{H}_{\xi=0}$, we can work out the expression by normal ordering it using Baker-Hausdorff (BH) formula. For deconfinement model, straightforward algebra gives

$$\begin{aligned}ig_d^{>}(x,t)&=\frac{a^{\frac{(v-1)^2}{2v}}}{2\pi}[i(x+vt)+a]^{-\frac{(v+1)^2}{4v}}\\&\quad\times[i(-x+vt)+a]^{-\frac{(v-1)^2}{4v}},\\ig_d^{<}(x,t)&=\frac{a^{\frac{(v-1)^2}{2v}}}{2\pi}[i(-x-vt)+a]^{-\frac{(v+1)^2}{4v}}\\&\quad\times[i(x-vt)+a]^{-\frac{(v-1)^2}{4v}},\end{aligned}\tag{B12}$$

where $v=\sqrt{1+g}$ with dimensionless coupling constant $g=ue^2/\pi$. For confinement model, it gives

$$ig_{\rm c}^{>}(x,t)=\frac{1}{2\pi a}\exp\left\{-\int_{2\pi/L}^{\infty}dqe^{-aq}\frac{m^4}{4q^2\varepsilon_q^{\rm c}}\left[\frac{1-e^{-i(qx+\varepsilon_q^{\rm c}t)}}{\left(\varepsilon_q^{\rm c}+q\right)^2}+\frac{1-e^{i(qx-\varepsilon_q^{\rm c}t)}}{\left(\varepsilon_q^{\rm c}-q\right)^2}\right]\right\},\tag{B13}$$

$$ig_{\rm c}^{<}(x,t)=\frac{1}{2\pi a}\exp\left\{-\int_{2\pi/L}^{\infty}dqe^{-aq}\frac{m^4}{4q^2\varepsilon_q^{\rm c}}\left[\frac{1-e^{i(qx+\varepsilon_q^{\rm c}t)}}{\left(\varepsilon_q^{\rm c}+q\right)^2}+\frac{1-e^{-i(qx-\varepsilon_q^{\rm c}t)}}{\left(\varepsilon_q^{\rm c}-q\right)^2}\right]\right\}.\tag{B14}$$

Then we can calculate the spectral functions using the Fourier transformation. The results are shown in Fig. 5, which exhibit linear dispersion in momentum space.

2. Gauge violation spectroscopy

Because of the orthogonality of states in different gauge sectors, the gauge violation correlations can be written

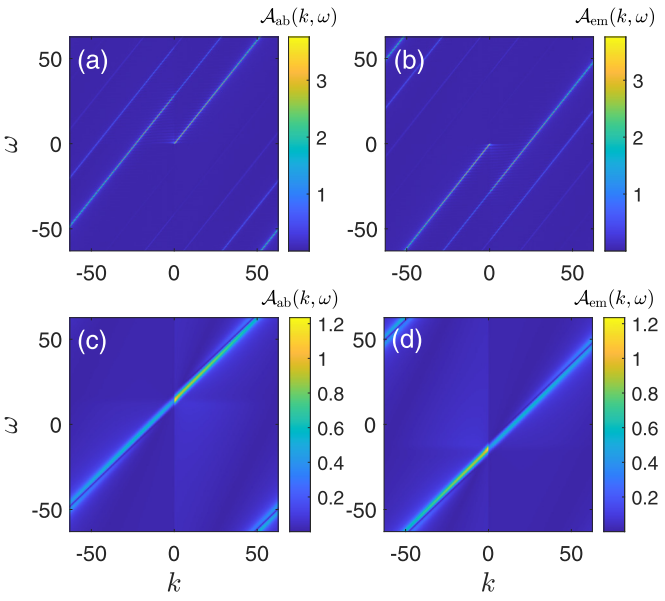

FIG. 5. The gauge invariance single-particle absorbing and emission spectrum for (a), (b) deconfinement model and (c), (d) confinement model. We have set coupling constant $g = 0.5$, the mass of boson $m = e/\sqrt{\pi} = 0.17$, and system size $L \to +\infty$.

as

$$ig_\sigma^>(x,t) = \delta(x)\langle\psi_0|\hat{\Psi}_R(0)e^{-i\hat{H}_\xi^\sigma t}\hat{\Psi}_R^\dagger(0)|\psi_0\rangle e^{+iE_0^\sigma t},$$
$$ig_\sigma^<(x,t) = \delta(x)\langle\psi_0|\hat{\Psi}_R^\dagger(0)e^{+i\hat{H}_\xi^\sigma t}\hat{\Psi}_R(0)|\psi_0\rangle e^{-iE_0^\sigma t}.$$

Substitute Eqs. (B8), (B11) into the above correlations, and we obtain

$$\begin{aligned} ig_\sigma^>(x,t) = \frac{\delta(x)}{2\pi a}\langle\psi_0|e^{+\sum_q[\eta_q^\sigma(0)\hat{\beta}_q^\dagger - \eta_q^{*\sigma}(0)\hat{\beta}_q]} \\ \times e^{-it\sum_q \varepsilon_q^\sigma(\hat{\beta}_q^\dagger+\xi h_q^{\sigma*})(\hat{\beta}_q+\xi h_q^\sigma)} \\ \times e^{-\sum_q[\eta_q^\sigma(0)\hat{\beta}_q^\dagger - \eta_q^{*\sigma}(0)\hat{\beta}_q]}|\psi_0\rangle e^{-i\xi^2\tilde{E}_Q^\sigma t}, \end{aligned}$$

and $ig_\sigma^<(x,t)$ is similar. Note that $e^{+\sum_q[\eta_q^\sigma(0)\hat{\beta}_q^\dagger - \eta_q^{*\sigma}(0)\hat{\beta}_q]}$ is a translation operator

$$e^{+\sum_q[\eta_q^\sigma(0)\hat{\beta}_q^\dagger - \eta_q^{\sigma*}(0)\hat{\beta}_q]}\hat{\beta}_q^\dagger e^{-\sum_q[\eta_q^\sigma(0)\hat{\beta}_q^\dagger - \eta_q^{\sigma*}(0)\hat{\beta}_q]} = \hat{\beta}_q^\dagger - \eta_q^{\sigma*},$$
$$e^{+\sum_q[\eta_q^\sigma(0)\hat{\beta}_q^\dagger - \eta_q^{\sigma*}(0)\hat{\beta}_q]}\hat{\beta}_q e^{-\sum_q[\eta_q^\sigma(0)\hat{\beta}_q^\dagger - \eta_q^{\sigma*}(0)\hat{\beta}_q]} = \hat{\beta}_q - \eta_q^\sigma.$$

Thus we obtain

$$ig_\sigma^>(x,t) = \frac{\delta(x)}{2\pi a}\langle\psi_0|e^{-it\sum_q \varepsilon_q^\sigma(\hat{\beta}_q^\dagger+\chi_q^{\sigma*})(\hat{\beta}_q+\chi_q^\sigma)}|\psi_0\rangle e^{-i\xi^2\tilde{E}_Q^\sigma t} \tag{B15}$$

with $\chi_q^\sigma = \xi h_q^\sigma - \eta_q^\sigma(0)$. Then, we can define $\hat{B}_q^\sigma = \hat{\beta}_q + \chi_q^\sigma$, such that $\hat{B}_q^\sigma|\psi_0\rangle = \chi_q^\sigma|\psi_0\rangle$. That is to say the ground state $|\psi_0\rangle$ in physical sector is the coherent state of operator $\hat{B}_q^\sigma$. Thus we have

$$\begin{aligned} ig_\sigma^>(x,t) &= \frac{\delta(x)}{2\pi a}\langle\psi_0|e^{-it\sum_q \varepsilon_q^\sigma \hat{B}_q^\dagger\hat{B}_q}|\psi_0\rangle e^{-i\xi^2\tilde{E}_Q^\sigma t} \\ &= \exp\left[-i\xi^2\tilde{E}_Q^\sigma t + \sum_q |\chi_q^\sigma|^2\left(e^{-i\varepsilon_q^\sigma t}-1\right)\right]. \end{aligned}$$

Now let us calculate the summation

$$\begin{aligned} \sum_q |\chi_q^\sigma|^2\left(e^{-i\varepsilon_q^\sigma t}-1\right) = \sum_{q>0}\frac{2\pi}{|q|L}\gamma_{q,\sigma}^+\left(e^{-i\varepsilon_q^\sigma t}-1\right) \\ + \sum_{q<0}\frac{2\pi}{|q|L}\gamma_{q,\sigma}^-\left(e^{-i\varepsilon_q^\sigma t}-1\right), \end{aligned}$$

where we have defined

$$\gamma_{q,\sigma}^+ = \left|1+\xi\sqrt{\frac{|q|L}{2\pi}}\frac{\lambda_q^\sigma}{\varepsilon_q^\sigma}(u_q^\sigma - v_q^\sigma)\right|^2,$$
$$\gamma_{q,\sigma}^- = \left|1+\xi\sqrt{\frac{|q|L}{2\pi}}\frac{\lambda_q^\sigma}{\varepsilon_q^\sigma}(v_q^\sigma - u_q^\sigma)\right|^2.$$

For the deconfinement model, $\gamma_{q,d}^{+,-}$ is independent of q because of the linearity of the dispersion relation $\varepsilon_q^d = \sqrt{1+g}|q|$. Thus, we can calculate the summation by using the formula $\ln(1-x) = -\sum_{n>0}x^n/n$, and the gauge violation correlations read

$$ig_d^>(x,t) = \frac{\delta(x)}{2\pi a}\left(\frac{-ia}{vt-ia}\right)^{\frac{v^2+1}{2v^3}}, \tag{B16}$$
$$ig_d^<(x,t) = \frac{\delta(x)}{2\pi a}\left(\frac{ia}{vt+ia}\right)^{\frac{v^2+1}{2v^3}}. \tag{B17}$$

For the confinement model, since $\gamma_{q,c}^{+,-}$ depends on q, it is hard to obtain a compact analytic form. Here, we only show the exponential integral

$$\begin{aligned} &ig_c^>(x,t) \\ &= \frac{\delta(x)}{2\pi a}\exp\left\{-\int_{2\pi/L}^\infty dq e^{-aq}\frac{m^4}{4q^2\varepsilon_q^c}\right. \\ &\left.\times\left[\frac{1-e^{-i\varepsilon_q^c t}}{(\varepsilon_q^c+q)^2}+\frac{1-e^{-i\varepsilon_q^c t}}{(\varepsilon_q^c-q)^2}\right]\right\} \\ &\times\exp\left\{+\int_{2\pi/L}^\infty dq e^{-aq}\frac{(q^2+\varepsilon_q^{c2})m^2}{2q^2\varepsilon_q^{c3}}\left(1-e^{-i\varepsilon_q^c t}\right)\right\}, \end{aligned} \tag{B18}$$

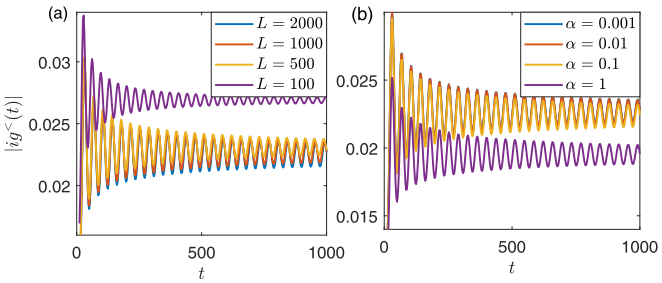

FIG. 6. The norm of the gauge violation Green's function of Schwinger model with $m = 0.17$. (a) Results for $L = 100, 500, 1000, 2000$, and $\alpha = 0.01$. (b) Results for $\alpha = 1, 0.1, 0.01, 0.001$, and $L = 1000$. We find $L = 1000$ and $\alpha = 0.01$ have converged the results.

$$ig_{\rm c}^{<}(x,t)=\frac{\delta(x)}{2\pi a}\exp\left\{-\int_{2\pi/L}^{\infty}dqe^{-aq}\frac{m^4}{4q^2\varepsilon_q^{\rm c}}\left[\frac{1-e^{i\varepsilon_q^{\rm c}t}}{\left(\varepsilon_q^{\rm c}+q\right)^2}+\frac{1-e^{i\varepsilon_q^{\rm c}t}}{\left(\varepsilon_q^{\rm c}-q\right)^2}\right]\right\}\exp\left\{+\int_{2\pi/L}^{\infty}dqe^{-aq}\frac{\left(q^2+\varepsilon_q^{\rm c2}\right)m^2}{2q^2\varepsilon_q^{\rm c3}}\left(1-e^{i\varepsilon_q^{\rm c}t}\right)\right\}. \tag{B19}$$

After the Fourier transformation, we obtain the gauge violation spectral functions as shown in the main text. Here $L=1000$ in Schwinger model, $L\to\infty$ in deconfinement model and $\alpha=0.01$ for all data have converged the results as illustrated in Fig. 6. In the case $m=0$ or $g=0$, the Schwinger-like models reduce to massless Dirac model. All results above are consistent with the known results in the particular case.

[1] S. Weinberg, *The Quantum Theory of Fields, Vol. 2: Modern Applications* (Cambridge University Press, Cambridge, 1995).

[2] J. Kogut, An introduction to lattice gauge theory and spin systems, Rev. Mod. Phys. **51**, 659 (1979).

[3] E. Fradkin, *Field Theories of Condensed Matter Physics* (Cambridge University Press, Cambridge, 2013).

[4] C. Schweizer, F. Grusdt, M. Berngruber, L. Barbiero, E. Demler, N. Goldman, I. Bloch, and M. Aidelsburger, Floquet approach to $\mathbb{Z}_2$ lattice gauge theories with ultracold atoms in optical lattices, Nature Phys. **15**, 1168 (2019).

[5] B. Yang, H. Sun, R. Ott, H.-Y. Wang, T. V. Zache, J. C. Halimeh, Z.-S. Yuan, P. Hauke, and J.-W. Pan, Observation of gauge invariance in a 71-site Bose-Hubbard quantum simulator, Nature (London) **587**, 392 (2020).

[6] A. Mil, T. V. Zache, A. Hegde, A. Xia, R. P. Bhatt, M. K. Oberthaler, P. Hauke, J. Berges, and F. Jendrzejewski, A scalable realization of local U(1) gauge invariance in cold atomic mixtures, Science **367**, 1128 (2020).

[7] Z.-Y. Zhou, G.-X. Su, J. C. Halimeh, R. Ott, H. Sun, P. Hauke, B. Yang, Z.-S. Yuan, J. Berges, and J.-W. Pan, Thermalization dynamics of a gauge theory on a quantum simulator, Science **377**, 311 (2022).

[8] J. Mildenberger, W. Mruczkiewicz, J. C. Halimeh, Z. Jiang, and P. Hauke, Probing confinement in a Z_2 lattice gauge theory on a quantum computer, arXiv:2203.08905.

[9] G.-X. Su, H. Sun, A. Hudomal, J.-Y. Desaules, Z.-Y. Zhou, B. Yang, J. C. Halimeh, Z.-S. Yuan, Z. Papić, and J.-W. Pan, Observation of many-body scarring in a Bose-Hubbard quantum simulator, Phys. Rev. Res. **5**, 023010 (2023).

[10] H.-Y. Wang, W.-Y. Zhang, Z.-Y. Yao, Y. Liu, Z.-H. Zhu, Y.-G. Zheng, X.-K. Wang, H. Zhai, Z.-S. Yuan, and J.-W. Pan, Interrelated thermalization and quantum criticality in a lattice gauge simulator, Phys. Rev. Lett. **131**, 050401 (2023).

[11] W.-Y. Zhang, Y. Liu, Y. Cheng, M.-G. He, H.-Y. Wang, T.-Y. Wang, Z.-H. Zhu, G.-X. Su, Z.-Y. Zhou, Y.-G. Zheng, H. Sun, B. Yang, P. Hauke, W. Zheng, J. C. Halimeh, Z.-S. Yuan, and J.-W. Pan, Observation of microscopic confinement dynamics by a tunable topological θ-angle, arXiv:2306.11794.

[12] E. A. Martinez, C. A. Muschik, P. Schindler, D. Nigg, A. Erhard, M. Heyl, P. Hauke, M. Dalmonte, T. Monz, P. Zoller, and R. Blatt, Real-time dynamics of lattice gauge theories with a few-qubit quantum computer, Nature (London) **534**, 516 (2016).

[13] N. Klco, E. F. Dumitrescu, A. J. McCaskey, T. D. Morris, R. C. Pooser, M. Sanz, E. Solano, P. Lougovski, and M. J. Savage, Quantum-classical computation of Schwinger model dynamics using quantum computers, Phys. Rev. A **98**, 032331 (2018).

[14] N. Klco, M. J. Savage, and J. R. Stryker, SU(2) non-Abelian gauge field theory in one dimension on digital quantum computers, Phys. Rev. D **101**, 074512 (2020).

[15] J. C. Halimeh and P. Hauke, Reliability of lattice gauge theories, Phys. Rev. Lett. **125**, 030503 (2020).

[16] J. C. Halimeh, V. Kasper, and P. Hauke, Fate of lattice gauge theories under decoherence, arXiv:2009.07848.

[17] J. C. Halimeh, L. Homeier, C. Schweizer, M. Aidelsburger, P. Hauke, and F. Grusdt, Stabilizing lattice gauge theories through simplified local pseudogenerators, Phys. Rev. Res. **4**, 033120 (2022).

[18] J. C. Halimeh, H. Lang, J. Mildenberger, Z. Jiang, and P. Hauke, Gauge-symmetry protection using single-body terms, PRX Quantum **2**, 040311 (2021).

[19] A. Smith, J. Knolle, D. L. Kovrizhin, and R. Moessner, Disorder-free localization, Phys. Rev. Lett. **118**, 266601 (2017).

[20] M. Brenes, M. Dalmonte, M. Heyl, and A. Scardicchio, Many-body localization dynamics from gauge invariance, Phys. Rev. Lett. **120**, 030601 (2018).

[21] A. Smith, J. Knolle, R. Moessner, and D. L. Kovrizhin, Dynamical localization in $\mathbb{Z}_2$ lattice gauge theories, Phys. Rev. B **97**, 245137 (2018).

[22] Z. Yao, C. Liu, P. Zhang, and H. Zhai, Many-body localization from dynamical gauge fields, Phys. Rev. B **102**, 104302 (2020).

[23] W. Zheng and P. Zhang, Floquet engineering of a dynamical Z_2 lattice gauge field with ultracold atoms, arXiv:2011.01500.

[24] J. C. Halimeh, L. Homeier, H. Zhao, A. Bohrdt, F. Grusdt, P. Hauke, and J. Knolle, Enhancing disorder-free localization through dynamically emergent local symmetries, PRX Quantum **3**, 020345 (2022).

[25] J. Osborne, I. P. McCulloch, and J. C. Halimeh, Disorder-free localization in 2+1D lattice gauge theories with dynamical matter, arXiv:2301.07720.

[26] M. Van Damme, J. C. Halimeh, and P. Hauke, Gauge-symmetry violation quantum phase transition in lattice gauge theories, arXiv:2010.07338.

[27] F. F. Assaad and T. Grover, Simple fermionic model of deconfined phases and phase transitions, Phys. Rev. X **6**, 041049 (2016).

[28] J. A. Sobota, Y. He, and Z.-X. Shen, Angle-resolved photoemission studies of quantum materials, Rev. Mod. Phys. **93**, 025006 (2021).

[29] Q. Chen, Y. He, C.-C. Chien, and K. Levin, Theory of radio frequency spectroscopy experiments in ultracold Fermi gases

and their relation to photoemission in the cuprates, Rep. Prog. Phys. **72**, 122501 (2009).

[30] J. T. Stewart, J. P. Gaebler, and D. S. Jin, Using photoemission spectroscopy to probe a strongly interacting Fermi gas, Nature (London) **454**, 744 (2008).

[31] C. H. Schunck, Y.-il Shin, A. Schirotzek, and W. Ketterle, Determination of the fermion pair size in a resonantly interacting superfluid, Nature (London) **454**, 739 (2008).

[32] P. Wang, Z.-Q. Yu, Z. Fu, J. Miao, L. Huang, S. Chai, H. Zhai, and J. Zhang, Spin-orbit coupled degenerate fermi gases, Phys. Rev. Lett. **109**, 095301 (2012).

[33] L. W. Cheuk, A. T. Sommer, Z. Hadzibabic, T. Yefsah, W. S. Bakr, and M. W. Zwierlein, Spin-injection spectroscopy of a spin-orbit coupled fermi gas, Phys. Rev. Lett. **109**, 095302 (2012).

[34] Z. Yan, P. B. Patel, B. Mukherjee, R. J. Fletcher, J. Struck, and M. W. Zwierlein, Boiling a unitary fermi liquid, Phys. Rev. Lett. **122**, 093401 (2019).

[35] A. Schirotzek, C.-H. Wu, A. Sommer, and M. W. Zwierlein, Observation of fermi polarons in a tunable fermi liquid of ultracold atoms, Phys. Rev. Lett. **102**, 230402 (2009).

[36] C. Kohstall, M. Zaccanti, M. Jag, A. Trenkwalder, P. Massignan, G. M. Bruun, F. Schreck, and R. Grimm, Metastability and coherence of repulsive polarons in a strongly interacting Fermi mixture, Nature (London) **485**, 615 (2012).

[37] F. Scazza, G. Valtolina, P. Massignan, A. Recati, A. Amico, A. Burchianti, C. Fort, M. Inguscio, M. Zaccanti, and G. Roati, Repulsive fermi polarons in a resonant mixture of ultracold ^{6}Li atoms, Phys. Rev. Lett. **118**, 083602 (2017).

[38] N. Jørgensen, L. Wacker, K. Skalmstang, M. Parish, J. Levinsen, R. Christensen, G. Bruun, and J. Arlt, Observation of attractive and repulsive polarons in a bose-einstein condensate, Phys. Rev. Lett. **117**, 055302 (2016).

[39] M.-G. Hu, M. Van de Graaff, D. Kedar, J. P. Corson, E. A. Cornell, and D. S. Jin, Bose polarons in the strongly interacting regime, Phys. Rev. Lett. **117**, 055301 (2016).

[40] C. Senko, J. Smith, P. Richerme, A. Lee, W. C. Campbell, and C. Monroe, Coherent imaging spectroscopy of a quantum many-body spin system, Science **345**, 430 (2014).

[41] P. Jurcevic, P. Hauke, C. Maier, C. Hempel, B. P. Lanyon, R. Blatt, and C. F. Roos, Spectroscopy of interacting quasiparticles in trapped Ions, Phys. Rev. Lett. **115**, 100501 (2015).

[42] P. Roushan, C. Neill, J. Tangpanitanon, V. M. Bastidas, A. Megrant, R. Barends, Y. Chen, Z. Chen, B. Chiaro, A. Dunsworth, A. Fowler, B. Foxen, M. Giustina, E. Jeffrey, J. Kelly, E. Lucero, J. Mutus, M. Neeley, C. Quintana, D. Sank *et al.*, Spectroscopic signatures of localization with interacting photons in superconducting qubits, Science **358**, 1175 (2017).

[43] J. Schwinger, Gauge invariance and mass. II, Phys. Rev. **125**, 397 (1962).

[44] J. Schwinger, Gauge invariance and mass, II, Phys. Rev. **128**, 2425 (1962).

[45] T. Giamarchi, *Quantum Physics in One Dimension* (Oxford University Press, Oxford, 2003).

[46] Y. Cheng, S. Liu, W. Zheng, P. Zhang, and H. Zhai, Tunable confinement-deconfinement transition in an ultracold atom quantum simulator, PRX Quantum **3**, 040317 (2022).

[47] J. C. Halimeh, I. P. McCulloch, B. Yang, and P. Hauke, Tuning the topological θ-angle in cold-atom quantum simulators of gauge theories, PRX Quantum **3**, 040316 (2022).

[48] F. M. Surace, P. P. Mazza, G. Giudici, A. Lerose, A. Gambassi, and M. Dalmonte, Lattice gauge theories and string dynamics in rydberg atom quantum simulators, Phys. Rev. X **10**, 021041 (2020).

[49] See Appendixes for bosonization of the Schwinger-like models (Appendix A). Calculation of gauge violation and gauge invariant spectral functions (Appendix B).